

Supporting Information

CO₂ hydrogenation to methanol and hydrocarbons over bifunctional Zn-doped ZrO₂/Zeolite catalysts

Pierfrancesco Ticali^{a†}, Davide Salusso^{a†}, Rafia Ahmad^b, Christian Ahoba-Sam^c, Adrian Ramirez^b, Genrikh Shterk^b, Kirill A. Lomachenko^d, Elisa Borfecchia^a, Sara Morandi^a, Luigi Cavallo^b, Jorge Gascon^{b*}, Silvia Bordiga^{a*}, Unni Olsbye^{c*}

^aDepartment of Chemistry, NIS Center and INSTM Reference Center, University of Turin, 10125, Turin, Italy.

^bKing Abdullah University of Science and Technology, KAUST Catalysis Center (KCC), Thuwal 23955, Saudi Arabia.

^cSMN Centre for Materials Science and Nanotechnology, Department of Chemistry, University of Oslo, N-0315 Oslo, Norway.

^dEuropean Synchrotron Radiation Facility, CS 40220, 38043 Grenoble Cedex 9, France.

[†]Authors equally contributed

1. Materials

H-ZSM-5 (SiO₂/Al₂O₃ = 23, S_{BET} = 417 m²/g) was purchased from Zeolyst. SAPO-34 (SiO₂/Al₂O₃ = 0.5, S_{BET} = 770 m²/g) was purchased from ACS materials. All the zeolites were dried at 120 °C for 12 h and calcined at 550 °C for 2 hours prior to testing.

2. Textural and structural characterization of the ZrZn-X catalysts

The N₂ adsorption/desorption isotherms and the pore size distributions (PSDs) of the as prepared ZrZn-X catalysts are displayed in Figure S1 and S2, respectively.

All samples exhibit the hysteresis loop due to the capillary condensation.¹ ZrZn-5 shows adsorption hysteresis different to that of ZrZn-15 and ZrZn-30. ZrZn-5 reveals a H2-like loop, which is characteristic of mesoporous oxides with tubular/ink-bottle pores featured by inhomogeneous dimension.² Conversely, ZrZn-15 and ZrZn-30 present a H1-like loop which is characteristic of mesoporous materials with narrow pore distribution and homogenous sized particles agglomerates,¹ typically spherical particles.

Nonetheless, it is worth notifying that there are not evidences concerning the origin of these porosity, indeed, it can be associated to either *inter-grains* pores, *intra-grains* pores, or both.

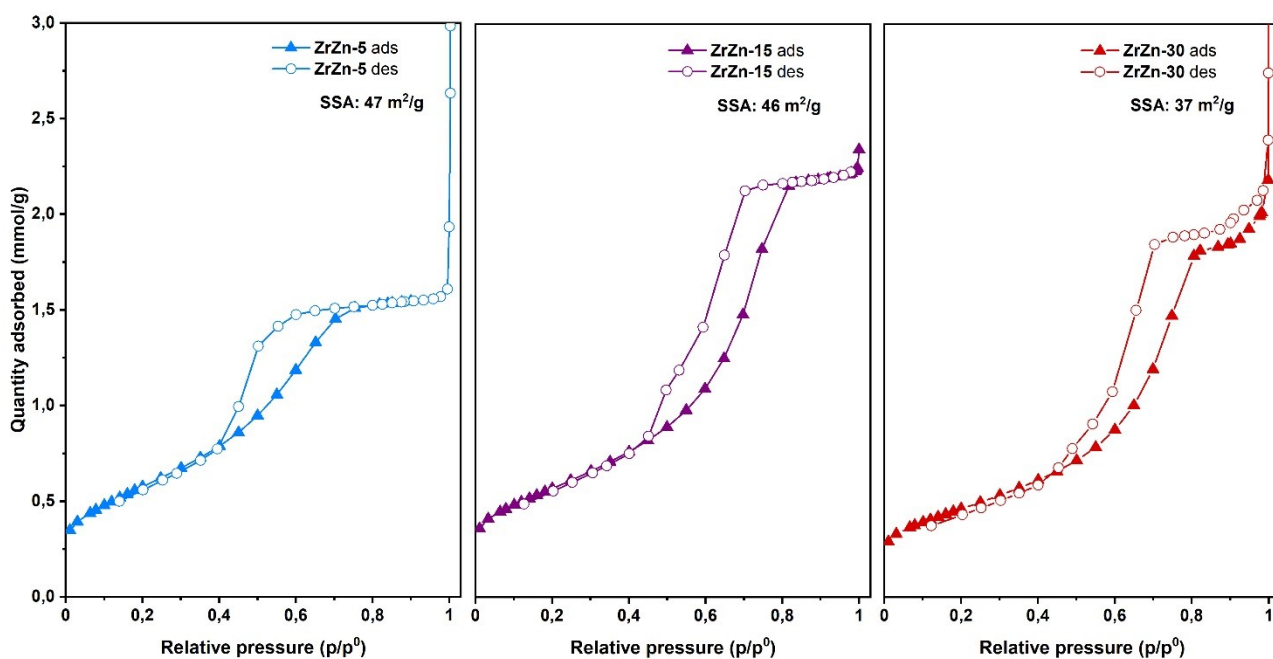


Figure S1. Adsorption/desorption isotherms of N_2 at 77 K for ZrZn-5, ZrZn-15 and ZrZn-30 catalysts.

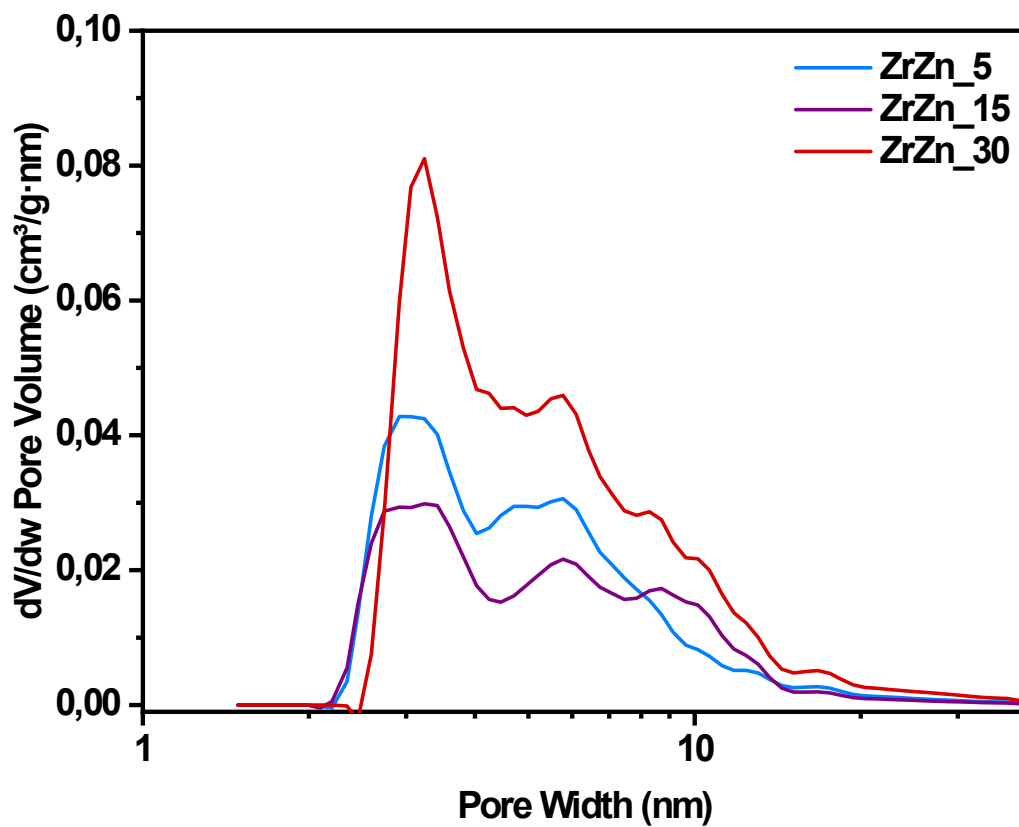


Figure S2. Pore size distribution of ZrZn-X catalysts, obtained by DFT method.

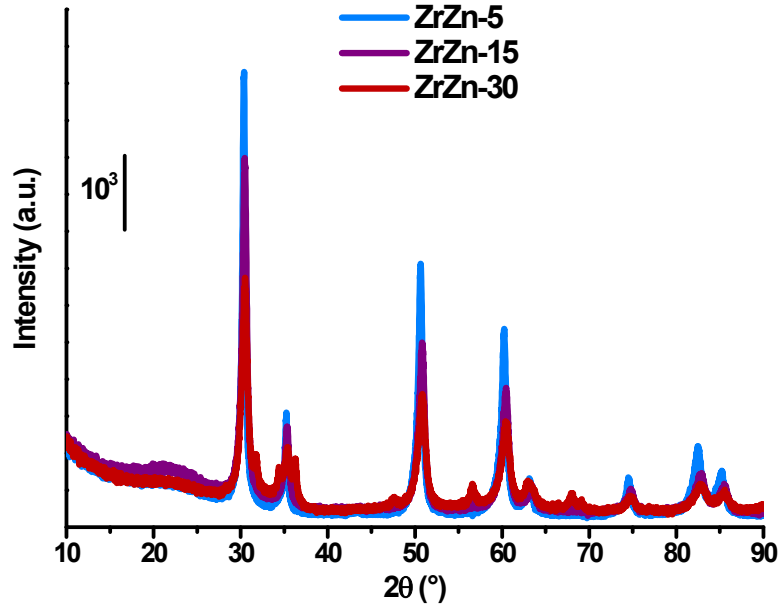


Figure S3. PXRD of the ZrZn-X catalysts collected at RT and shown in the full 2θ -range. Offset shift of the three diffractograms was not applied.

Lattice parameters, crystallite sizes and phase wt.% resumed in Table S2 were extracted by Rietveld refinement method³ implemented in the FullProf-suite⁴ programme package. Scale factor, lattice parameters and background were refined in this order. Background was modelled using a linear interpolation of more than 30 points. Crystallite size is extracted from the Full Width Half Maximum (FWHM) with the well-known Debye-Scherrer equation:

$$\langle D \rangle = \frac{0.94\lambda}{L * \cos\theta} \quad (\text{S1})$$

where $\langle D \rangle$ is the average crystallite size, L the peak FWHM and λ the used wavelength. The FWHM is extracted from the peak only once its profile has been modelled. To model the peak profile, we used the Thompson-Cox Hastings (TCH)⁵ Pseudo Voigt function. This function mimics the Voigt function where instrumental and sample broadening are described by a convolution of Gaussian and Lorentzian contributions. Their FWHM H_G and H_L are respectively described as:

$$H_G = (U \tan^2\theta + V \tan\theta + W + I_G \cos\theta)^{1/2} \quad (\text{S2})$$

where U , V and W are the Caglioti's instrumental parameters (Eq. S4), while I_G is related to the size broadening:

$$H_L = X \tan\theta + Y / \cos\theta + Z \quad (\text{S3})$$

where Y is related to the size broadening while X and Z to the strain contribution to broadening.

The instrumental contribution to the broadening is described by the Caglioti's formula (Eq. S4),⁶ which is contained in the Gaussian contribution to FWHM:

$$H = (U \tan^2 \theta + V \tan \theta + W)^{1/2} \quad (\text{S4})$$

where U, V and W are instrumental contributions obtained by measuring the standard reference material 640c Si from the National Institute of Technology (NIST) that shows a minimal amount of physical line broadening caused by defects (i.e. strain) and crystallite size.

I_G and Y parameters in eqs. S2, S3 were refined in order to obtain the best fit of the peak shape. X and Z were also refined, however as they are related to the strain contribution to the broadening, their further application is not discussed. I_G and Y are used in the TCH formula to calculate two new parameters, Z_s and η_s . Z_s is the FWHM from the crystallite size broadening while η_s mixes the Gaussian and Lorentzian functions. In the TCH formula, Z_s and η are expressed as series expansions:

$$Z_s^5 = I_G^{5/2} + 2.69269 I_G^2 Y + 2.42843 I_G^{3/2} Y^2 + 4.47163 I_G Y^3 + 0.07842 I_G^{1/2} Y^4 + Y^5$$

$$\eta_s = 1.36603 \frac{Y}{Z_s} - 0.47719 \left(\frac{Y}{Z_s} \right)^2 + 0.11116 \left(\frac{Y}{Z_s} \right)^3 \quad (\text{S5})$$

From this expression it becomes clear that η_s is not related to any physical parameter, therefore it is preferred to use H_G and H_L from eqs. S2, S3 in the fitting procedure since they are easily identified to particle-size effect, instrumental resolution and strain broadening.

Finally, under the Pseudo-Voigt approximation, average crystallite size is given by the expression derived from the Scherrer formula:

$$\langle D \rangle = \frac{\eta_s + (1 - \eta_s) \sqrt{\pi * \ln 2}}{Z_s} * \frac{360\lambda}{\pi^2} \quad (\text{S6})$$

Table S1 - Structural parameters of ZrZn-X catalysts obtained from PXRD Rietveld refinement, also including the ZnO extra-phase observed for ZrZn-30.

	ZrZn-5	ZrZn-15	ZrZn-30
ZrO₂			
Space group	P 4 ₂ /n m c	P 4 ₂ /n m c	P 4 ₂ /n m c
a (=b) (Å)	3.6049 ± 0.0008	3.58900 ± 0.00018	3.5944 ± 0.0008
c (Å)	5.0980 ± 0.0015	5.1020 ± 0.0005	5.082 ± 0.002
Crystallite size (nm)	55±1	20±1	12±1
Wt. %	100	100	85
ZnO			
Space group	/	/	P 6 ₃ mc
a (=b) (Å)	/	/	3.25109 ± 0.00019
c (Å)	/	/	5.2122 ± 0.0005
Wt. %	0	0	15

Table S2 - Structural parameters of tested ZrZn-30 catalyst obtained from PXRD Rietveld refinement.

	ZrO₂	ZnO
Space group	P 4 ₂ /n m c	P6 ₃ mc
<i>a</i> (=b) (Å)	3.5943±0.0009	3.25134±0.00018
<i>c</i> (Å)	5.087±0.003	5.2060±0.0005
Crystallite size (nm)	15±1	/
Wt.%	88	12

3. Spectroscopic characterization of the ZrZn-X catalysts

Figure S4 compares the spectra recorded in oxygen and in hydrogen at 400 °C for the three catalysts. As reported in the main text, for all the samples in both the conditions, absorption bands in the regions 4000-3000 cm⁻¹, 2500-2000 cm⁻¹ and 1700-1000 cm⁻¹, related to surface hydroxyls, CO₂ encapsulated in closed porosity and carbonate/nitrate species, respectively, are present. Reasonably, encapsulated CO₂ (¹²CO₂ and ¹³CO₂ bands at 2340 and 2210 cm⁻¹, respectively) carbonates and nitrates come from the precursors used during the preparation. These species, which despite the calcination at 500 °C are still present in all samples, are very evident even after oxidation and reduction at 400 °C. It is worth to note that the amount of surface hydroxyls decreases on increasing Zn content.

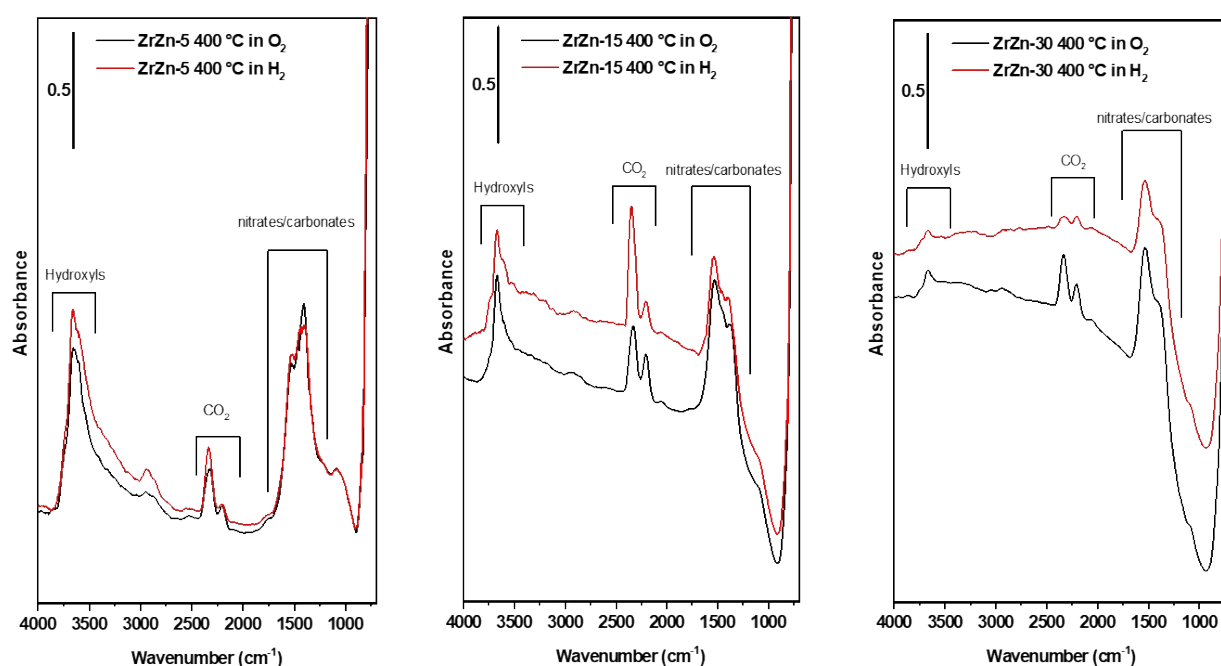


Figure S4. FT-IR spectra of ZrZn-X catalysts recorded at 400 °C in 40 mbar of oxygen (black curves) and 40 mbar of hydrogen (red curves).

4. Molecular modelling of the ZrZn-X catalysts

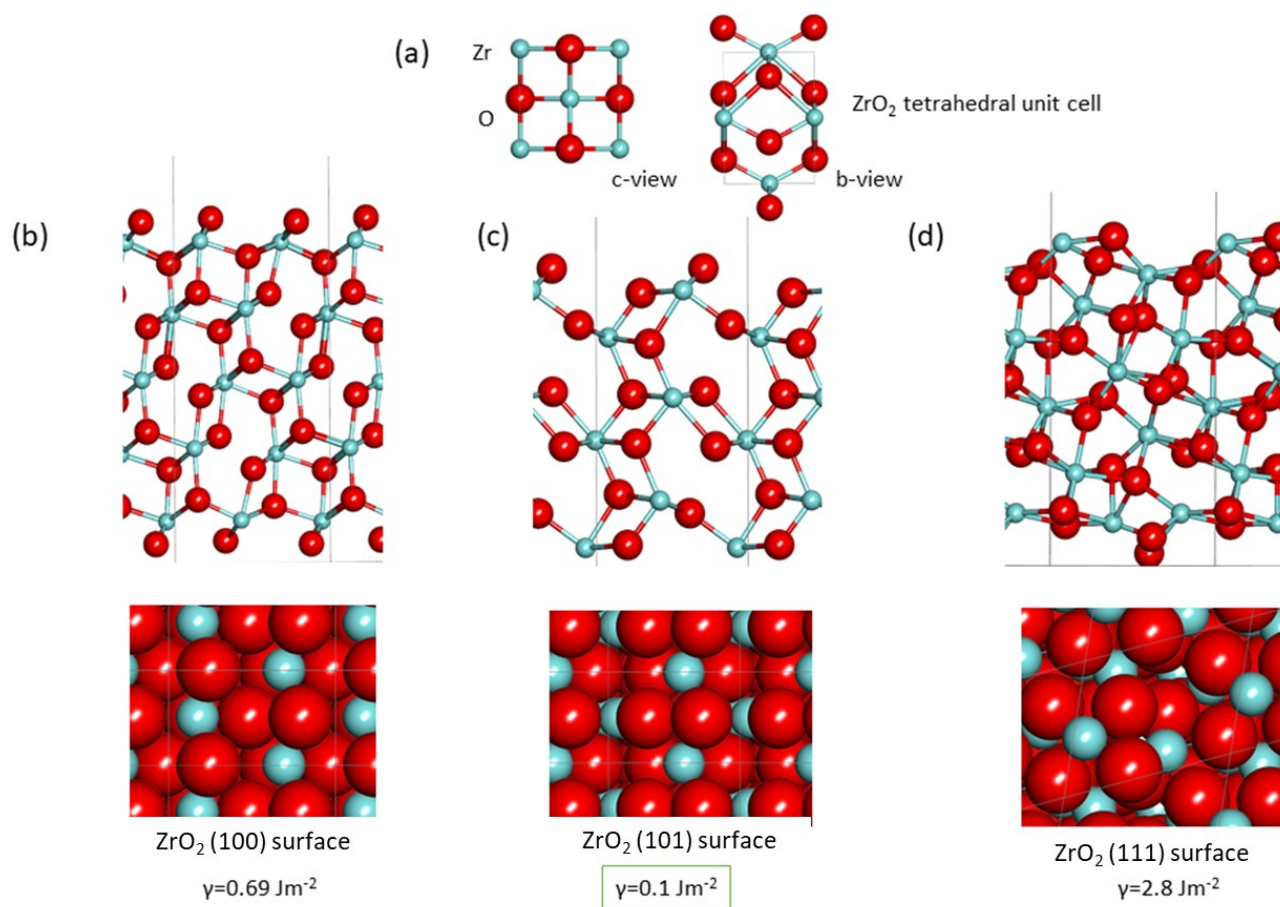


Figure S5. (a) Completely optimized unit cell of a tetrahedral ZrO₂. Ball ‘n stick and space filling atoms representation for completely optimized (b) (100), (c) (101), and (d) (111) surfaces. The red and blue colors represent oxygen and zirconium atoms, respectively.

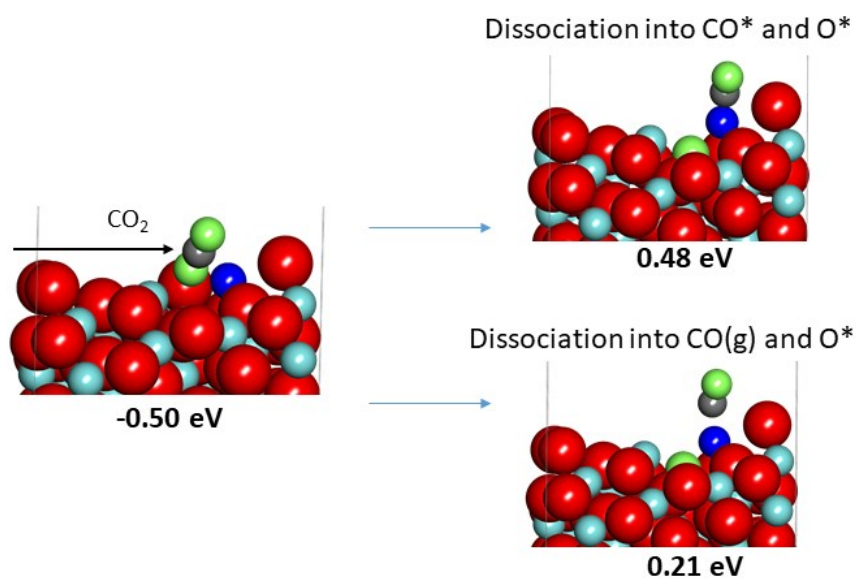


Figure S6. (a) Adsorption and consecutive dissociation of CO₂ on Zn-doped ZrO₂ (101) surface. The red, grey, blue and dark blue colors represent oxygen, carbon, zirconium and zinc atoms, respectively.

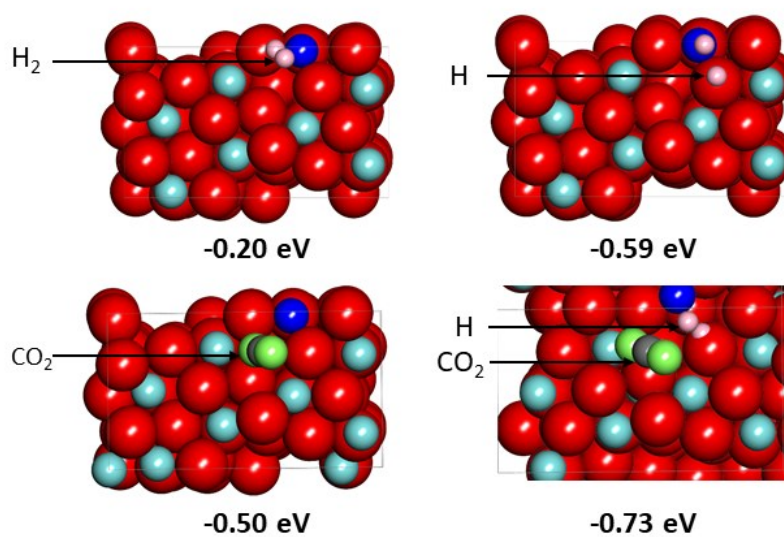


Figure S7. Adsorption of (a) H₂, (b) 2H, (c) CO₂, and (d) CO₂ + 2H on Zn-doped ZrO₂ (101) surface. The red, grey, blue and dark blue colors represent oxygen, carbon, zirconium and zinc atoms, respectively.

5. Testing results

5.1 Testing results on combined ZrZn-X/SAPO-34 system

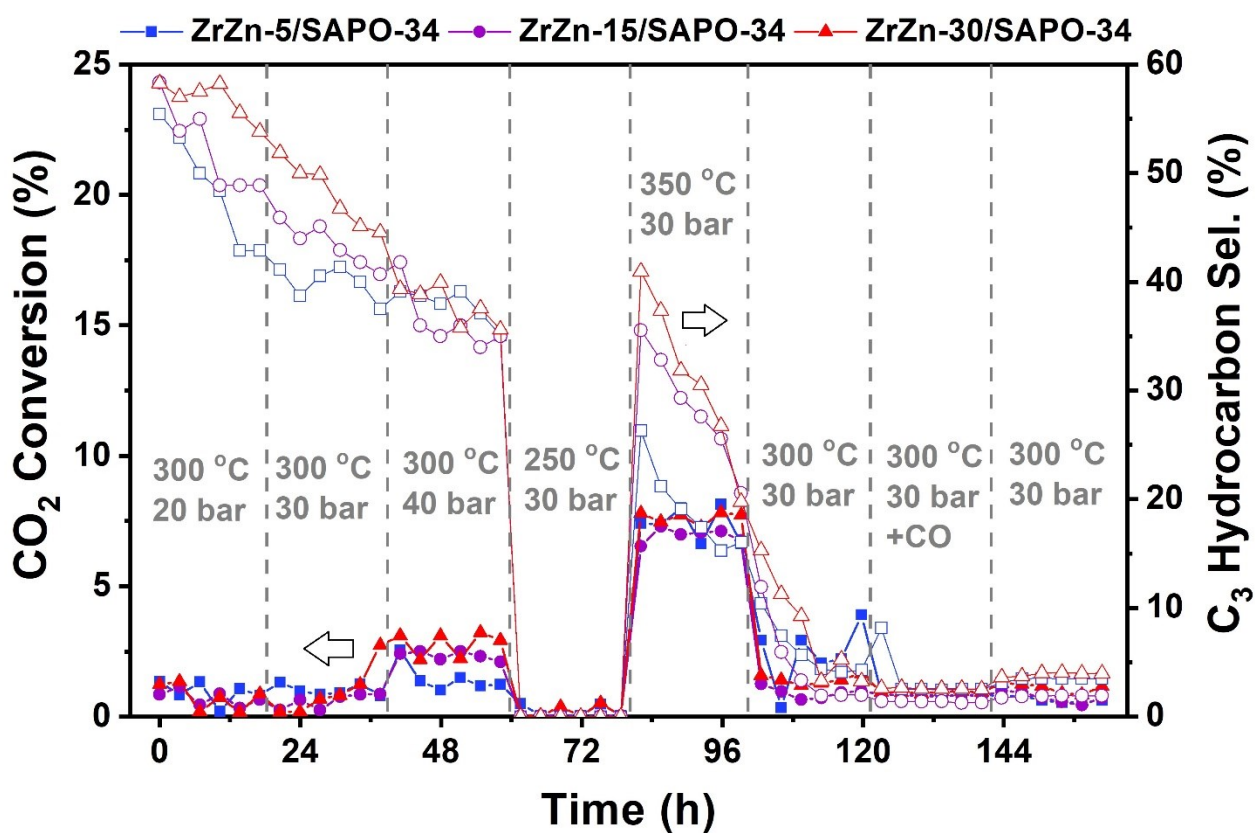


Figure S8. Catalytic performance of the combined ZrZn-X/SAPO-34 systems for the CO₂ conversion to hydrocarbons. CO₂:H₂ 1:3, 12000 mL/h/g. Please note that the secondary Y axis refers to the C₃ selectivity among hydrocarbons (CO free).

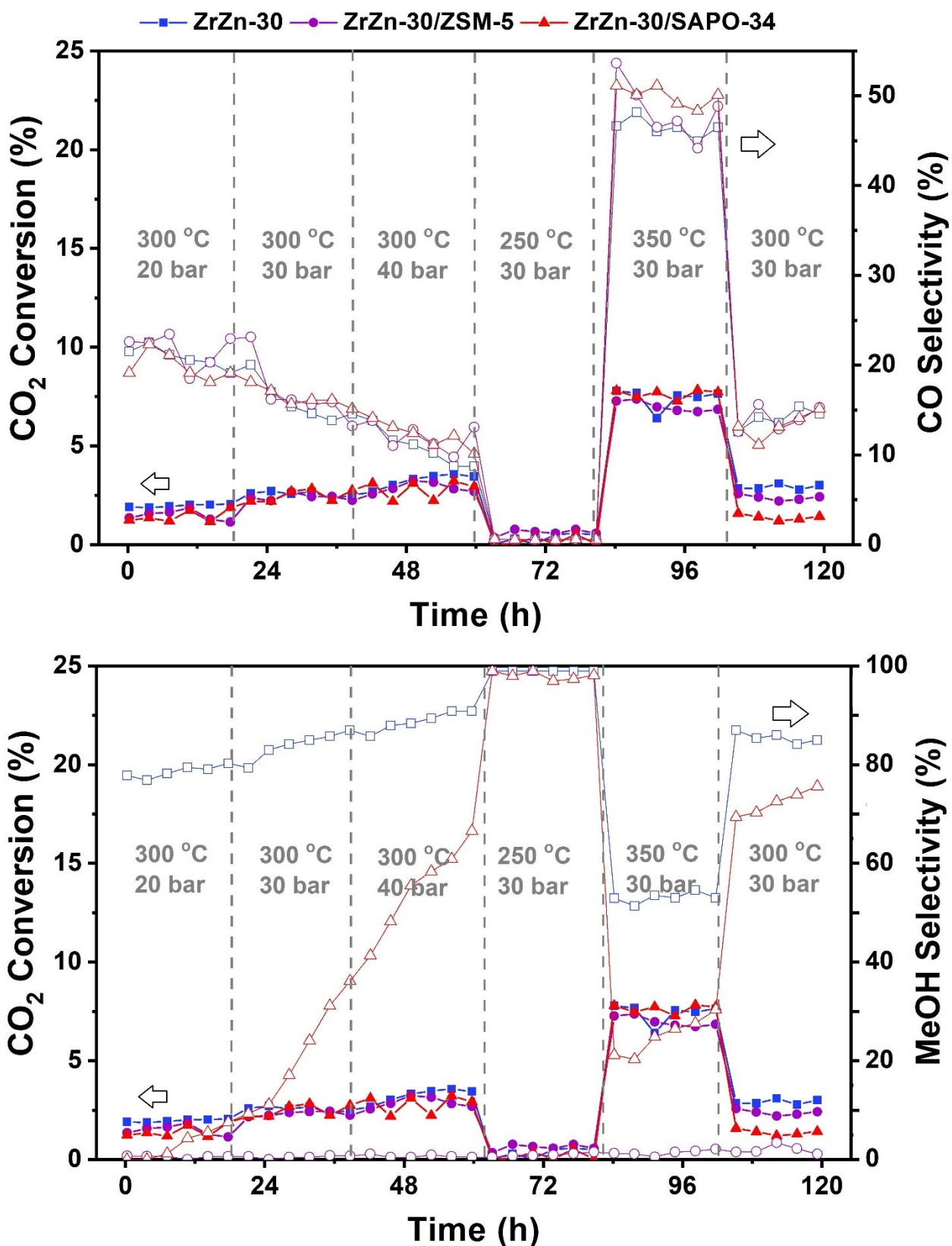


Figure S9. Comparison of the catalytic performance of the stand-alone ZrZn-30 and the combined ZrZn-30/SAPO-34 and ZrZn-30/ZSM-5 systems for the CO₂ conversion to hydrocarbons. CO₂:H₂ 1:3, 12000 mL/h/g.

5.2 Details on hydrocarbon distribution for ZrZn-30/ZSM-5 system

Table S3. Hydrocarbon distribution of the ZrZn-30/ZSM-5 combined system for the CO₂ conversion to hydrocarbons at different space times. CO₂:H₂ 1:3, 350 °C, 30 bars.

GHSV (ml/h/g)	C1	C2=	C2	C3=	C3	C4=	C4	C5=	C5	C6=	C6
24000	3.33	4.44	10.54	5.83	19.97	1.11	21.64	2.77	18.72	1.66	9.99
12000	3.13	6.61	12.71	10.18	18.80	3.13	16.19	2.61	15.67	1.57	9.40
6000	2.56	8.59	15.51	14.00	16.77	5.08	9.28	3.56	13.10	3.08	7.84

5.3 Testing results on ZrZn-30 alone and mixed with ZSM-5 at 350 °C, 30 bar, CO₂/H₂/Ar=2/6/1

The tests reported in this section were performed using a Microactivity E μ unit built by PID Eng& Tech (Micromeritics). The unit is equipped with a high-speed servo-controlled needle valve which allows for precise and stable control of pressure from 1 to 100 bar. A stainless steel flowreactor (6mmI.D) was used for the tests. The catalysts (ZrZn-30 as described in the Experimental section of the main manuscript, and H-ZSM-5 (Si/Al=25, purchased from Zeolyst International and Si/Al = 360, purchased from ACS materials)) were tested in ZrZn-30:ZSM-5 = 1:0 or 1:1 weight ratio with CO₂/H₂/inert flow ratio = 2/6/1 (τ = 0.0020-0.044 gcat min mL⁻¹) at 30 bar and 350 °C. The e μ luent from the reactor was analyzed with an online GC (Agilent 8890 equipped with one TCD and 2 FIDs, with a methanizer coupled to one of the FIDs to analyze both CO_x and oxygenates on one column using one detector). The catalysts were pretreated *in situ* at 400 °C in H₂ flow for 1 hr before testing.

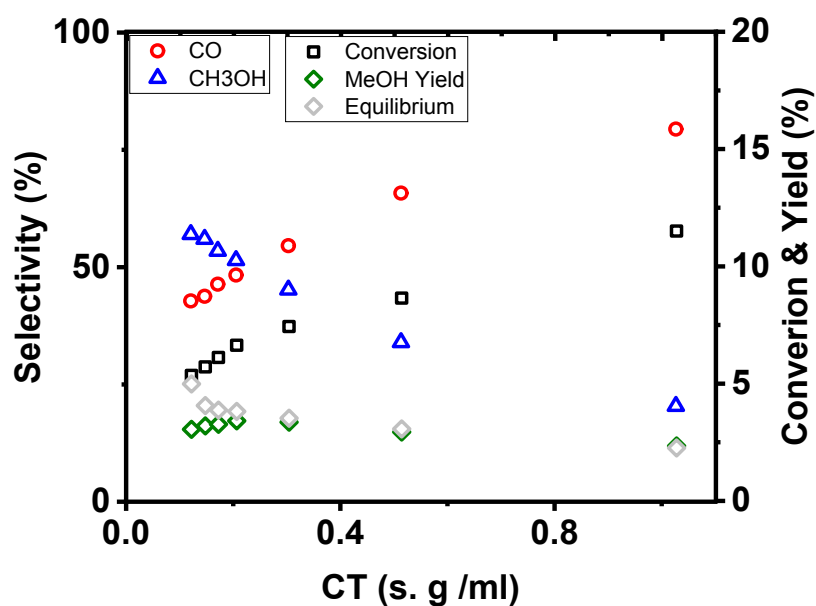


Figure S10. CO₂ conversion, product selectivity and methanol yield versus contact time over ZrZn-30, at 350 °C, 30 bar, CO₂:H₂:Inert = 2:6:1. Equilibrium methanol yield, taking into account water formed in the reverse water gas shift reaction, is shown as grey diamonds.

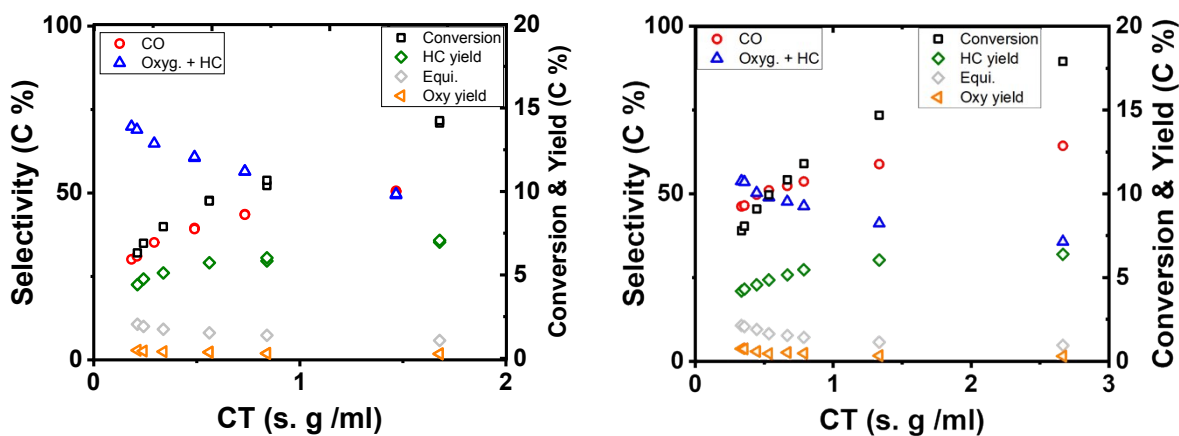


Figure S11. CO₂ conversion, product selectivity and methanol yield versus contact time over ZrZn-30 mixed in 1:1 weight ratio with ZSM-5 with Si/Al ratio of 25 (left) and Si/Al ratio of 360 (right), at 350 °C, 30 bar, CO₂:H₂:Inert = 2:6:1. Equilibrium methanol yield, taking into account water formed with CO and hydrocarbons, is shown as grey diamonds.

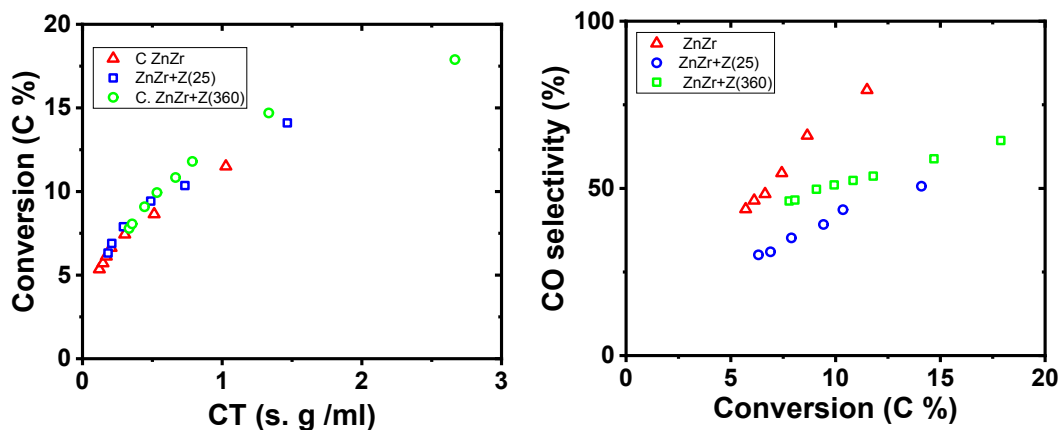


Figure S12. CO₂ conversion versus time on stream (left) and CO selectivity versus CO₂ conversion (right) for ZrZn-30 alone and mixed with ZSM-5 with Si/Al = 25 or 360, at at 350 °C, 30 bar, CO₂:H₂:Inert = 2:6:1.

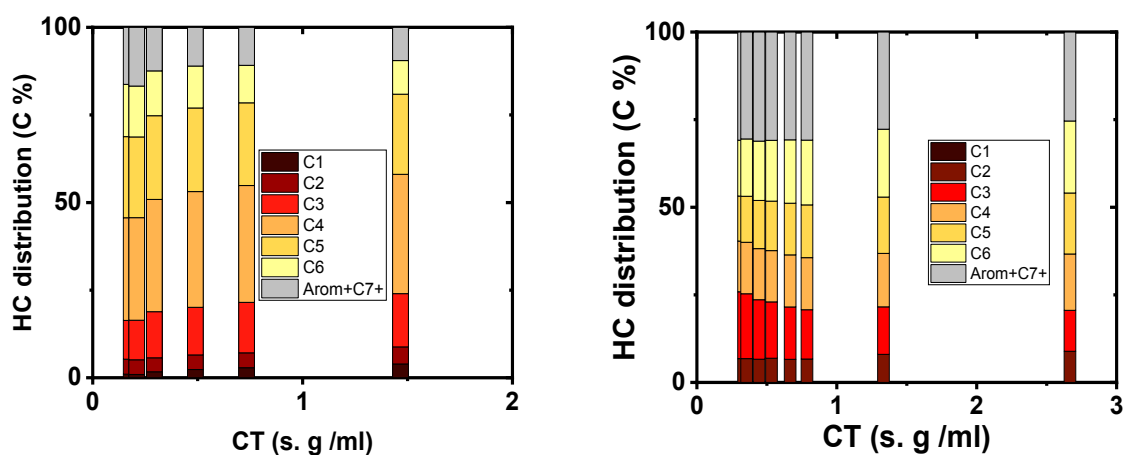


Figure S13. Hydrocarbon distribution versus contact time for ZrZn-30 mixed with ZSM-5 with Si/Al = 25 (left) or 360 (right), at at 350 °C, 30 bar, CO₂:H₂:Inert = 2:6:1.

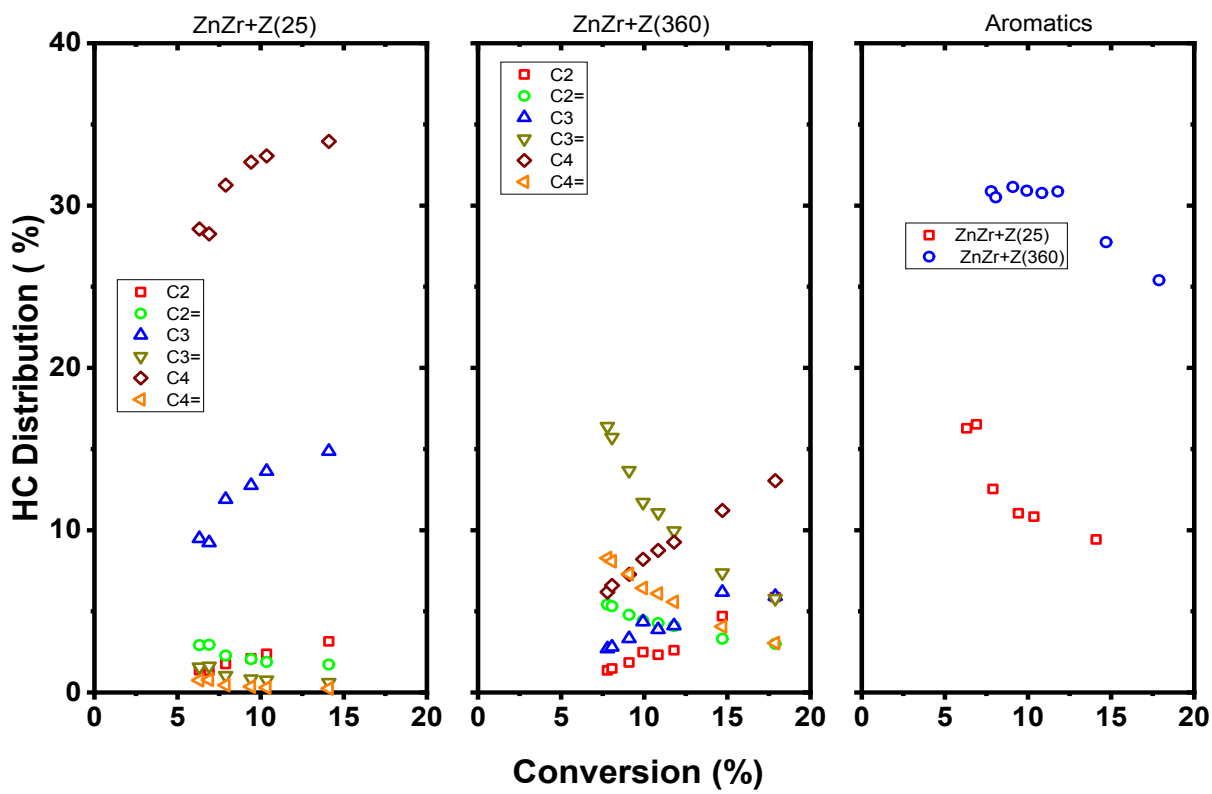


Figure S14. Hydrocarbon distribution versus CO₂ conversion for ZrZn-30 mixed with ZSM-5 with Si/Al = 25 or 360, at 350 °C, 30 bar, CO₂:H₂:Inert = 2:6:1.

6. XAS measurements on the combined ZrZn-X/ZSM-5 systems

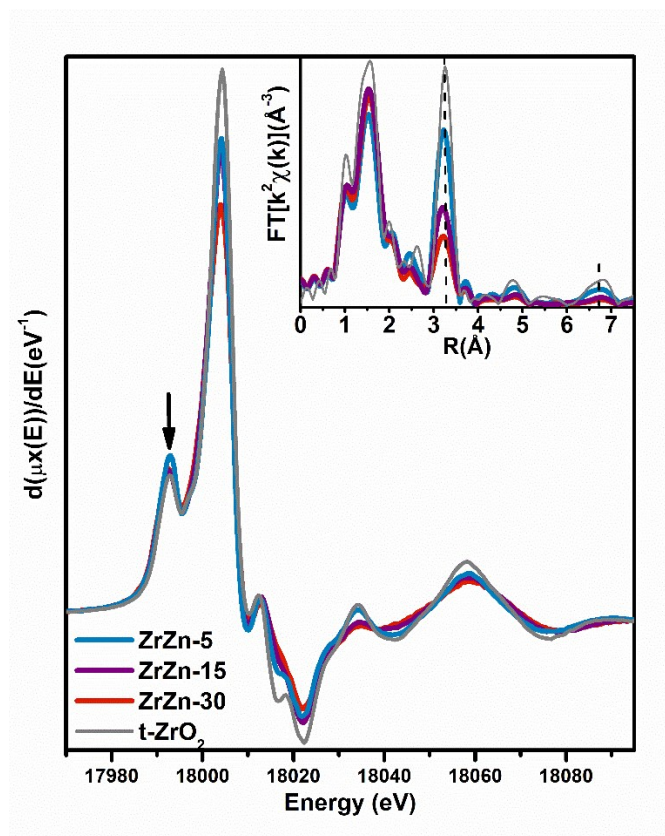


Figure S15. First derivative of the Zr K-edge XANES spectra collected at RT of the three catalysts (ZrZn-5/15/30) and of t-ZrO₂. Arrow in the main panel points the $1s \rightarrow 4d$ transition in the pre-edge. Dashed lines in the inset indicate respectively Zr-Zr second shell (around 3.3 \AA) and collinear multiple scattering (around 6.7 \AA). The EXAFS spectra reported in the inset have been obtained transforming the corresponding $k^2\chi(k)$ EXAFS functions in the 2.5-13 \AA^{-1} range.

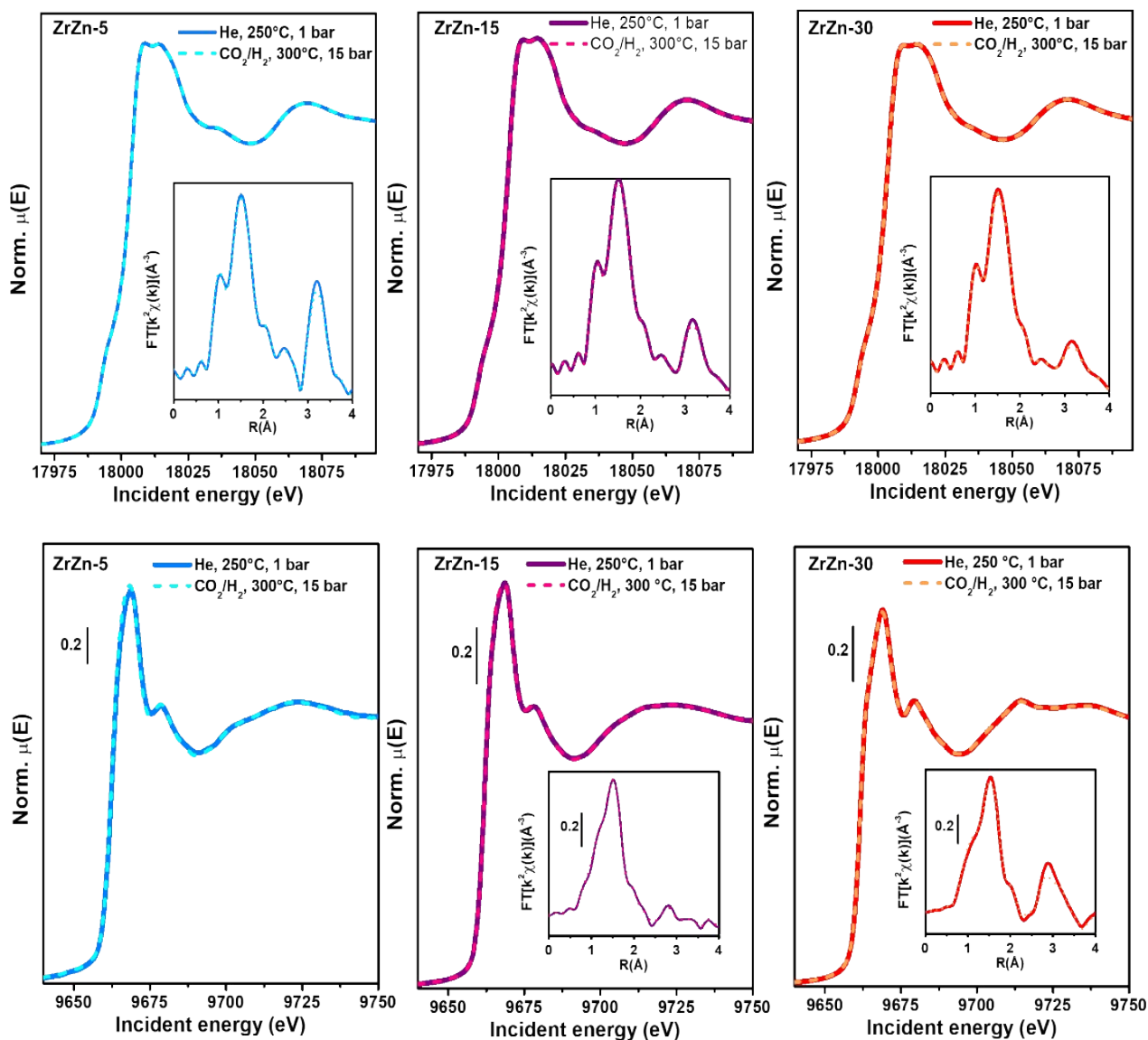


Figure S16. Operando Zr (top panels) and Zn (bottom panels) K-edge XANES (main panels) and FT-EXAFS (insets) of the three ZrZn-X/ZSM-5 combined system i) at 250 °C, 1 bar, He flow, after activation in H₂ up to 400 °C and just prior to exposure to reaction feed (solid lines); ii) under reaction conditions (300 °C, 15 bar, CO₂/H₂/He flow) (dashed lines). The EXAFS spectra reported in the insets have been obtained transforming the corresponding $k^2\chi(k)$ EXAFS functions in the 2.5-13 Å⁻¹ range.

7. Scanning electron microscopy

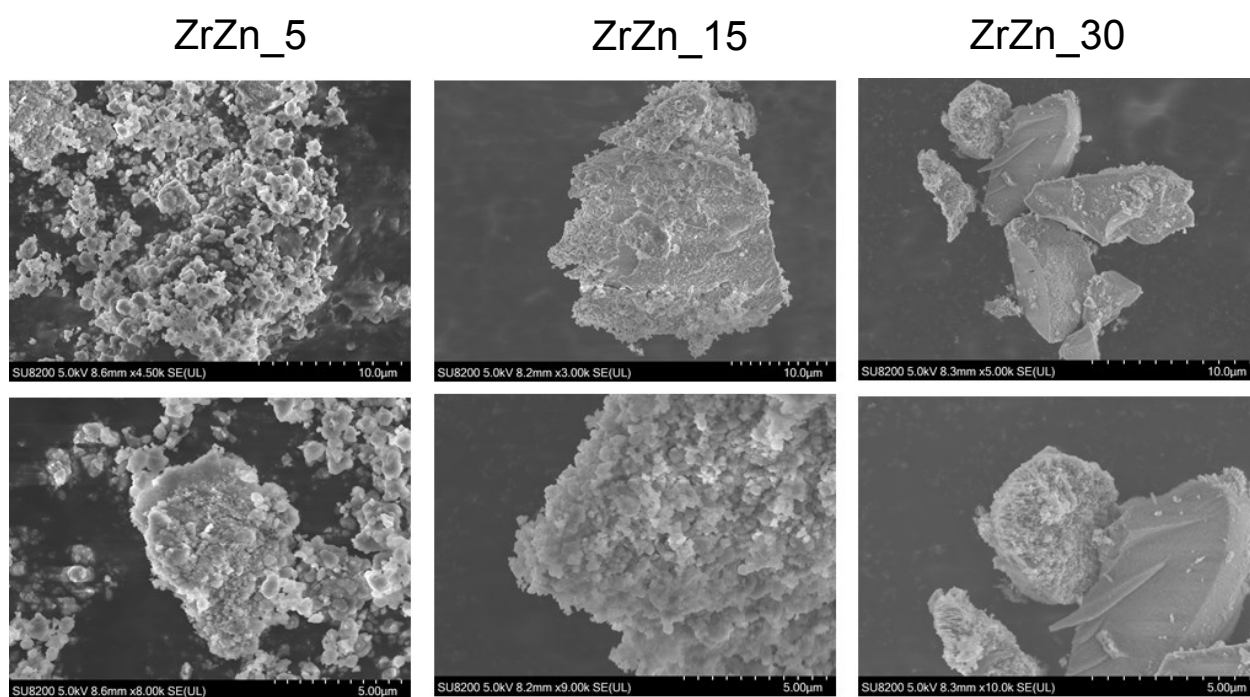


Figure S17. SEM images of representative ZrZn-X catalysts. The SEM images were taken on a Hitachi SU8230 Field Emission Scanning Electron Microscope.

8. X-ray photoelectron spectroscopy

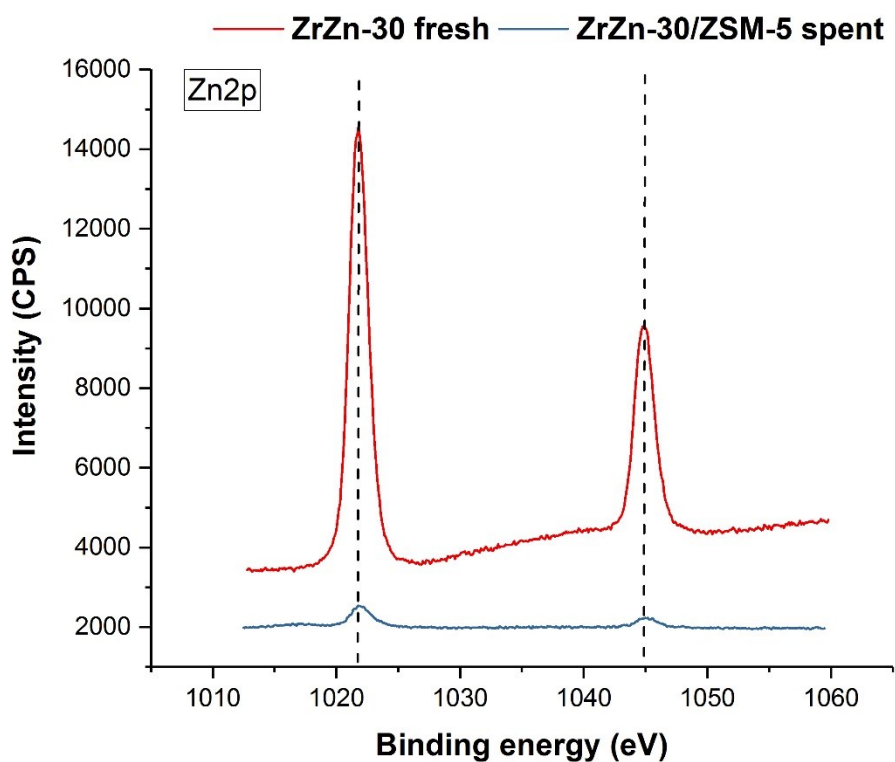


Figure S18. X-ray photoelectron spectroscopy of the fresh ZrZn-30 and spent ZrZn-30/ZSM-5 catalyst at the Zn2p level.

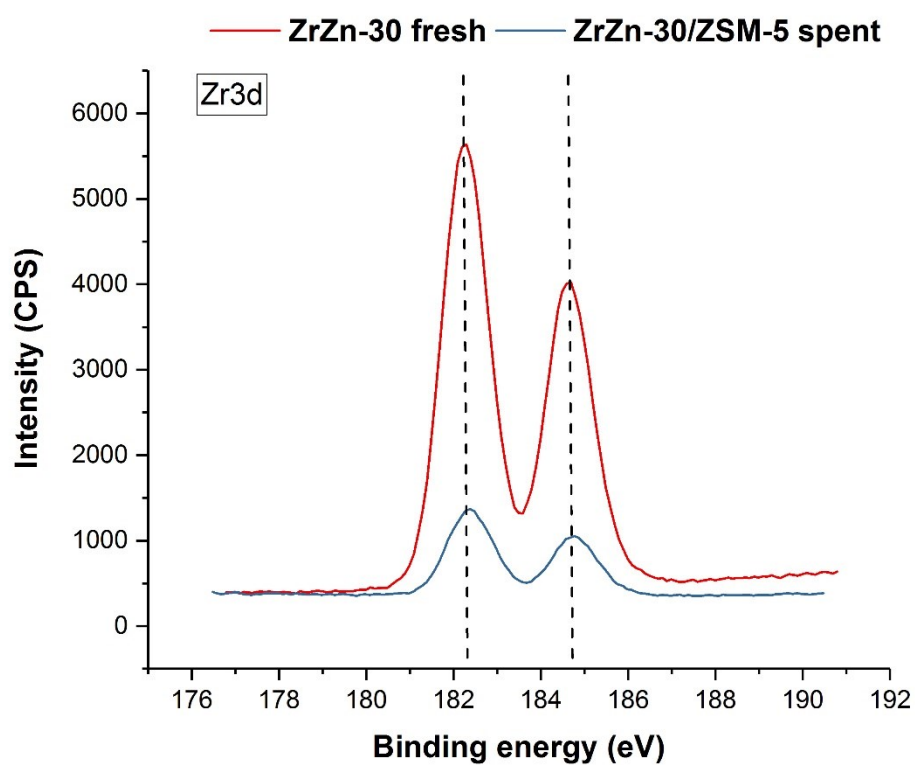


Figure S19. X-ray photoelectron spectroscopy of the fresh ZrZn-30 and spent ZrZn-30/ZSM-5 catalyst at the Zr3d level.

9. Transmission electron microscopy

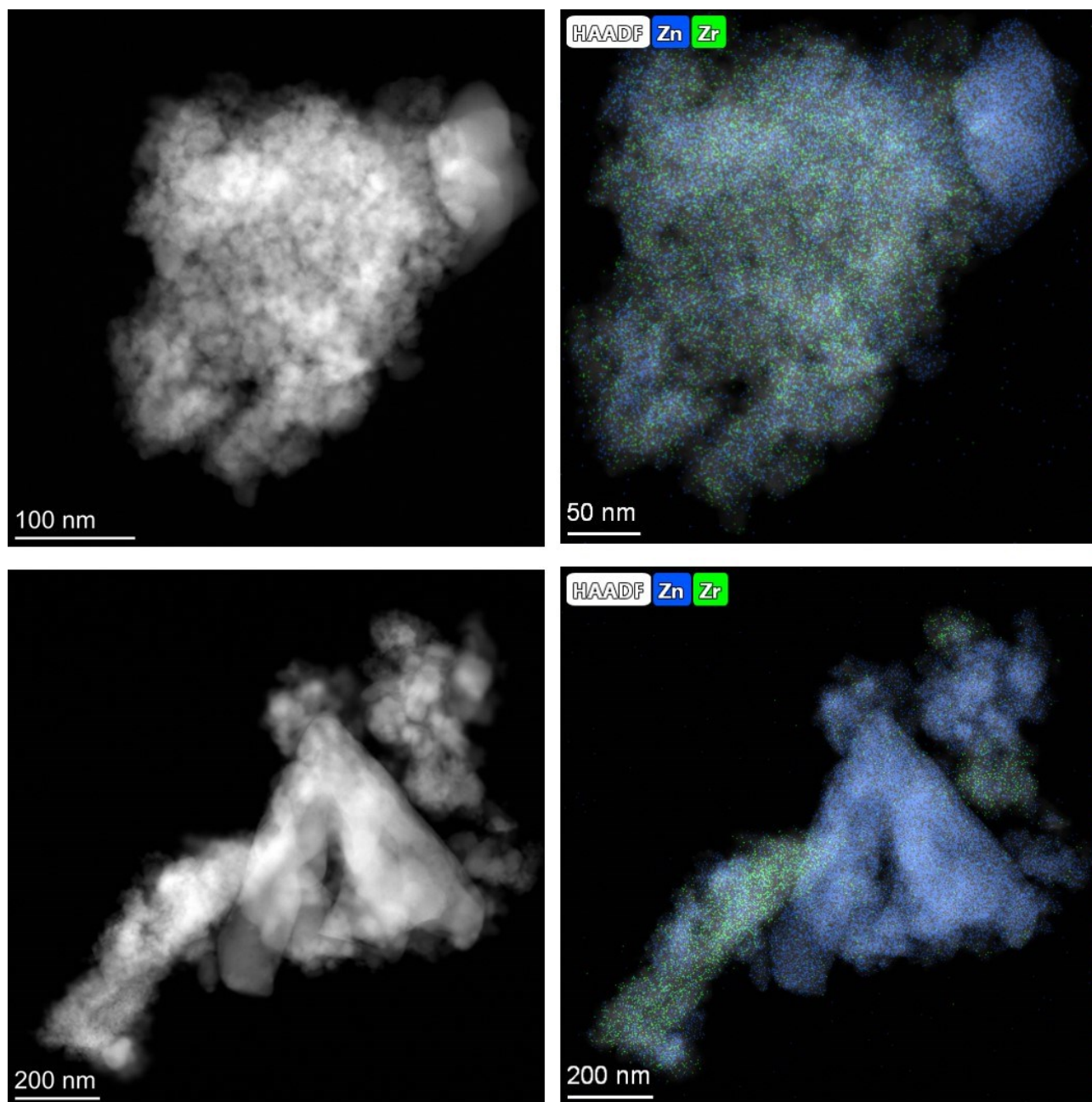


Figure S20. HAADF STEM-EDXS images of the fresh ZrZn-30 catalyst.

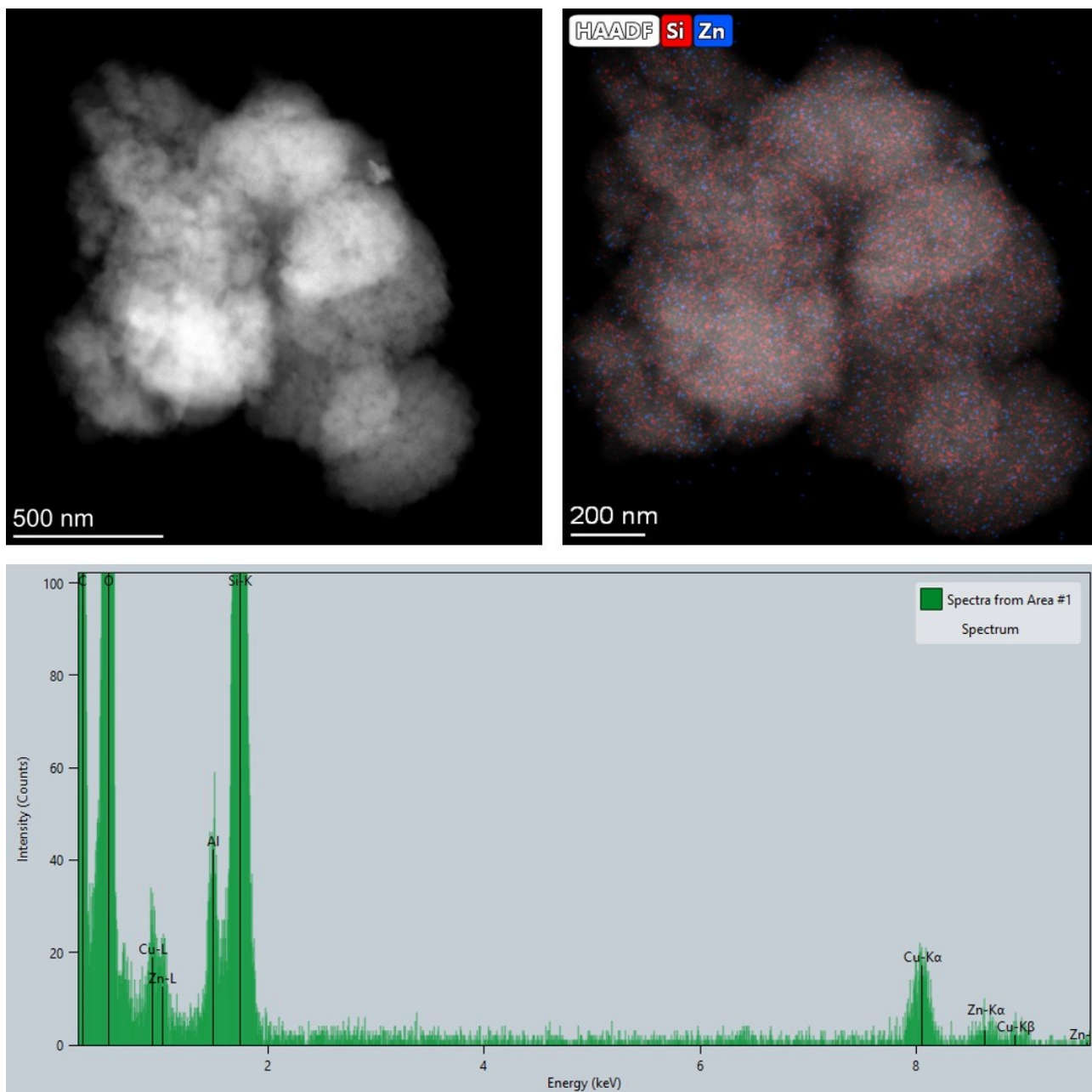


Figure S21. HAADF STEM-EDXS images and atomic spectra of the ZSM-5 zeolite component in the spent ZrZn-30/ZSM-5 catalyst after 48 hours in the reaction stream.

References

1. Sing, K. S. W. *et al.* Reporting Physisorption Data for Gas/Solid Systems with Special Reference to the Determination of Surface Area and Porosity. *Pure Appl. Chem.* **57**, 603–619 (1985).
2. Sing, K. S. W. & Williams, R. T. Physisorption hysteresis loops and the characterization of nanoporous materials. *Adsorpt. Sci. Technol.* **22**, 773–782 (2004).
3. Rietveld, H. M. A profile refinement method for nuclear and magnetic structures. *J. Appl. Crystallogr.* **2**, 65–71 (1969).
4. Rodríguez-Carvajal, J. Recent Developments of the Program Fullprof. *News. Comm. Powder Diffr. IUCr* **26**, 12–19 (2001).
5. Thompson, P. Cox D. E. and Hastings, J. B. Rietveld Refinement of Debye-Scherrer Synchrotron X-ray Data from Al₂O₃. *J. Appl. Crystallogr.* **20**, 79–83 (1987).
6. Caglioti G. *et al.* Choice of collimators for a crystal spectrometer for neutron diffraction. *Nucl. Instruments* **3**, 223–228 (1958).